The Correlation between X-Ray Line Ionization and Optical Spectral Types of the OB Stars

Nolan R. Walborn

Space Telescope Science Institute[1], 3700 San Martin Drive, Baltimore, MD 21218, USA

walborn@stsci.edu

Joy S. Nichols

Harvard-Smithsonian Center for Astrophysics, 60 Garden Street, Cambridge, MA 02138

jnichols@cfa.harvard.edu

Wayne L. Waldron

Eureka Scientific, Inc., 2452 Delmer Street, Suite 100, Oakland, CA 94602

wwaldron@satx.rr.com

ABSTRACT

Marked correlations are reported between the ionization of the X-ray line spectra of normal OB stars, as observed by the *Chandra X-Ray Observatory*, and their optical spectral types. These correlations include the progressive weakening of the higher ionization relative to the lower ionization X-ray lines with advancing spectral type, and the similarly decreasing intensity ratios of the H-like to He-like lines of the α ions. These relationships were not predicted by models, nor have they been clearly evident in astrophysical studies of a few objects; rather, they have emerged from morphological analysis of an adequate (albeit still small) sample, from which known peculiar objects such as magnetic stars and very rapid rotators have been isolated to reveal the normal trends. This process is analogous to that which first demonstrated the strong relationships between the UV wind profiles and the optical spectral types of normal OB stars, which likely bear a physical as well as a historical connection to the present X-ray results. Since the optical spectral types are calibrated in terms of fundamental stellar parameters,

---

it follows that the winds and X-ray spectra are determined by the latter. These observations provide strong guidance for further astrophysical modeling of these phenomena.

Subject headings: stars: early-type — stars: fundamental parameters — stars: winds — X-rays: stars

1. Introduction

When a new observational domain, comprising a diverse phenomenology not yet fully explained or predicted by physical models, is opened to investigation, the science of morphology may provide a useful initial formulation. For instance, morphology can discern empirical trends, separate the normal (majority) behavior from peculiar exceptions, reveal correlations with other kinds of information, and suggest or eliminate hypotheses for subsequent physical analysis, all with a minimum of prior assumptions. A frequent occurrence of this situation in astronomy is access to a new wavelength region or data of higher information content. A specific example from the relatively recent past is the extensive database of high-resolution ultraviolet stellar spectra generated by the *International Ultraviolet Explorer* (*IUE*) satellite. During the early 1980's, there was a debate about the relationship if any of OB stellar winds to the fundamental stellar parameters. A majority of specialists believed that it was weak or nonexistent, because of the large scatter in plots of mass-loss rate versus effective temperature or luminosity; however, it is now known that the derivations of those quantities were inadequate at that time. The debate was settled by a purely morphological demonstration of the detailed correlations between the wind profiles in the *IUE* data and the optical spectral types, which had in turn been calibrated in terms of fundamental parameters (Walborn et al. 1985, 1995, 2009; Rountree & Sonneborn 1991, 1993; Penny et al. 1996). The database provided by the *Far Ultraviolet Spectroscopic Explorer* (*FUSE*) supported the extension of those correlations to the rich spectral region below Lyman-α (Walborn et al. 2002, Pellerin et al. 2002). Of course, morphology does not explain anything, but it may pave the way toward the ultimate objective of physical understanding.

The *Chandra* (and *XMM-Newton*) X-ray satellites have provided the first stellar spectroscopic data of adequate quality to investigate the systematics of that regime. The samples remain small to date because the required high-resolution data are time-consuming to acquire with those systems. Nevertheless, they are sufficient for an initial morphological survey, which is presented here based on the *Chandra* data, with results that may be surprising.

2.   Observations

All of the observations were obtained with the *Chandra* Advanced CCD Imaging Spectrometer (ACIS) in its High Energy Transmission Grating Spectrometer (HETGS) configuration, which in turn simultaneously provides Medium Energy Grating (MEG) and High Energy Grating (HEG) data. The resolving powers are 660 at 15 Å and 1000 at 12.4 Å, respectively. We have combined the two datasets whenever possible, i.e., whenever the HEG S/N was adequate. The data discussed here were obtained from the TGCat (Huenemoerder et al. 2009) web-based catalog of *Chandra* grating data. TGCat processing starts with the Level 1 event data downloaded from the *Chandra* archive. Updated calibrations and responses are applied to the data and the zeroth order position is determined to high accuracy. The resulting TGCat Level 2 extracted spectral data were used to create the plots shown here.

Most of the data discussed here were archival and all are also available from the XATLAS web site (see Westbrook et al. 2008). Three of the four targets observed in our *Chandra* program (PI Waldron, ID 6200204) to fill gaps in the archival coverage of the HR Diagram are included here. They are HD 93250, 9 Sgr, and 15 Mon; our fourth target, HD 93129AB, presents a complex, composite spectrum that will be discussed separately (Nichols et al., in preparation.) Stellar and observational parameters are listed in Table 1, in the order in which the objects appear in Figures 1–6, together with extensive references to previous analyses of these stars. Further explanation of several columns in the table is given below.

3.   Results

The 5–25 Å X-ray spectra of 14 normal OB stars (or binary systems) are shown in order of advancing optical spectral types in Figures 1 and 2, which contain primarily main-sequence stars and supergiants, respectively, albeit with a few giants included to augment the coverage in each case. In these plots, each X-ray spectrogram has been scaled to 1.0 at the peak emission feature. Thus, absolute intensities cannot be directly compared between different objects, although line ratios can be. Because of the large range of line intensities in the calibrated data, a complementary presentation of the same data, but with three different scalings at wavelengths below 11 Å, from 11 to 18 Å, and above 18 A is given in Figures 3 and 4. The three normalization factors for each object are listed in Table 1; their units are photons s^{-1} cm^{-2} $Å^{-1}$. The largest of the three values (usually the third, except for three of the earliest types where it is the second) applies to Figures 1 and 2. As indicated by the spectral types, several objects are known close binaries. Parameters of the strong spectral lines are listed in Table 2.

Several correlations between the X-ray line ionization and the optical spectral types are immediately apparent in these figures. First, in Figures 1 and 2, the higher ionization, shorter wavelength lines weaken markedly relative to the lower ionization, longer wavelength lines in a given spectrum along the sequences, although the oxygen lines are usually the strongest. Second, in Figures 3 and 4, the behaviors of individual lines and line ratios, particularly those of the close pairs of lines from the H-like and He-like α ions, display strong trends along the sequences. Specifically, S XV essentially disappears after O3.5 on the main sequence, and after O4 in the supergiants. The Si XIV/Si XIII and Mg XII/Mg XI ratios diminish drastically between O3.5 and O4 in both sequences. The Ne X/Ne IX ratio is the best diagnostic, because it is the most sensitive throughout this spectral-type range. Unfortunately, the Ne X feature is blended with an Fe XVII line that strengthens toward the later types (as do the other lines from the latter ion), interfering with the visual trend; this blend is elucidated at a larger scale in Figure 5. Finally, the O VIII/O VII trend is relatively weak throughout this range, although the ratio reverses between the extreme cases of HD 150136 and β Cru (the spectrogram of HD 93250 has lower S/N and is unreliable at the longer wavelengths). The large N/O ratios in ζ Pup and ξ Per are most likely abundance effects in processed material, as previously derived in the former spectrum by Kahn et al. (2001); see also Oskinova et al. (2006). Note that the *differential* behaviors of the ionization ratios are themselves an ionization effect, with the intermediate Ne lines providing the best response to the relevant parameter range. Quantitative measurements (and corresponding uncertainties) of these line ratios, as well as the implied temperatures, are given by Waldron & Cassinelli (2007); note the revised values in the erratum to that paper. We present measurements of the Ne ratios below.

It is noteworthy that the binary nature of several objects, which may have colliding winds, does not interfere with these observed trends, although it may contribute to some of the scatter in them. Neither does the light to moderate range of interstellar extinctions among them (Table 1), for which no correction has been made here. The seven stars with E(B-V) between 0.3 and 0.5 are expected to have emission features longward of 18 Å extincted by factors up to 2–3. One might be concerned that the earlier type normal stars tend to have the higher interstellar extinctions, but ζ Pup provides the counterexample with an early type and low extinction that fits the X-ray line sequence well. Of course, wind or interstellar extinction always affects the longer wavelengths more, so it cannot cause the relatively weaker high ionization features at the later types. Neither would it affect the ratios of the close pairs of H-like to He-like lines significantly.

The present sample is not adequate to investigate luminosity effects in detail, but there are a few suggestive indications of an ionization correlation with that dimension as well. As noted above, the S XV line persists to a slightly later type in the supergiants. More systematically, it can be seen that the Si XIV and Mg XII lines remain stronger at later types

in the supergiants than on the main sequence (see also Waldron & Cassinelli 2007). Indeed, ι Ori rather breaks these trends in Figure 3, which may well be due to its giant nature. More extensive coverage of intermediate luminosity classes with X-ray data of this quality is required to determine whether these effects correlate in detail with that dimension.

Figure 6 displays the X-ray spectra of two magnetic and two very rapidly rotating OB stars. It is easily seen that they have much higher ionizations than those of normal stars with the same spectral types. They undoubtedly correspond to energetic circumstellar activity related to the fields or rotation (see also Wojdowski & Schulz 2005, Zhekov & Palla 2007, Westbrook et al. 2008). This result emphasizes once again that it is essential to eliminate pathological cases from the samples, if one intends to investigate the normal phenomena.

To summarize and somewhat quantify our results, we have measured the optimal Ne ratio, by means of Gaussian fits to the lines. Since the Ne x blend with the Fe xvii 12.124 Å line cannot be resolved, we have corrected for it approximately by measuring the isolated Fe xvii 15.014 Å line and subtracting it, scaled by the theoretical intensity ratio of 0.13, from the blend. The resultant Ne ratios are listed in Table 1 and plotted versus spectral type in Figure 7, with the luminosity classes and the peculiar objects distinguished by different symbols; the trends described above are well shown.

4. Discussion

The systematic characteristics of OB X-ray spectra just described have not emerged clearly from previous studies. The likely reasons are inadequate samples contaminated by peculiar objects, and the uncertainties of current physical models for the phenomena. As recounted in the Introduction, the situation regarding the systematics of OB stellar winds during the early 1980's was remarkably similar, and it was substantially illuminated by purely morphological investigations. In fact, the mass-loss rates and physical details of OB winds remain uncertain today, with the roles of clumping, rotation, and possibly weak magnetic fields being actively investigated. Nevertheless, the purely empirical descriptions of the phenomena stand as guides and objectives for the modeling.

The facts that the UV wind and X-ray spectral morphologies both correlate with the optical spectral types is likely no coincidence. Indeed, the X-rays most likely originate in the winds, and the observed correlations indicate that the detailed wind structures must be well determined by the fundamental stellar parameters, likely via the intense radiation fields of the OB stars. Waldron & Casinelli (2007) measured and analyzed several parameters in the X-ray spectra of nearly the same sample discussed here. The complexities they discuss are

impressive, e.g., the lines considered here must form at different depths in the winds and are thus subject to differing amounts of internal extinction. X-ray emission from shocks related to clumps distributed throughout the winds is discussed by Feldmeier et al. 2003, Oskinova et al. (2004, 2006), Zhekov & Palla (2007), Cassinelli et al. (2008), and Waldron & Cassinelli (2009). There may also be global asymmetric wind structures even in the normal stars, e.g., two-component equatorial vs. polar winds related to rotation and/or magnetic fields, as explored by Mullan & Waldron (2006). Nevertheless, the global correlations evident in the emergent spectra strongly suggest that all of these effects must be correlated and determined by the stellar and wind parameters. This result in turn provides strong guidance for further physical modeling of the winds and X-ray generation.

This conclusion may appear surprising, yet it was foreshadowed by the strong correlation between the bolometric and X-ray luminosities of the OB stars that has been known for many years (e.g., Sana et al. 2006). Moreover, several of the objects with peculiar X-ray spectra, such as those in Figure 7, deviated from that correlation (e.g., Cassinelli et al. 1994, Cohen et al. 1997). Of course, further physical modeling that uniquely reproduces the morphological correlations is required in order to understand them.

REFERENCES

Burkholder, V., Massey, P., & Morrell, N. 1997, ApJ, 490, 328

Cassinelli, J.P., Cohen, D.H., Macfarlane, J.J., Sanders, W.T., & Welsh, B.Y. 1994, ApJ, 421, 705

Cassinelli, J.P., Ignace, R., Waldron, W.L., Cho, J., Murphy, N.A., & Lazarian, A. 2008, ApJ, 683, 1052

Cassinelli, J.P., Miller, N.A., Waldron, W.L., MacFarlane, J.J., & Cohen, D.H. 2001, ApJ, 554, L55

Cohen, D.H., Cassinelli, J.P., & Macfarlane, J.J. 1997, ApJ, 487, 867

Cohen, D.H., de Messières, G.E., MacFarlane, J.J., Miller, N.A., Cassinelli, J.P., Owocki, S.P., & Liedahl, D.A. 2003, ApJ, 586, 495

Cohen, D.H., Kuhn, M.A., Gagné, M., Jensen, E.L.N., & Miller, N.A. 2008, MNRAS, 386, 1855

Cohen, D.H., Leutenegger, M.A., Grizzard, K.T., Reed, C.L., Kramer, R.H., & Owocki, S.P. 2006, MNRAS, 368, 1905

Donati, J.-F., Babel, J., Harries, T.J., Howarth, I.D., Petit, P., & Semel, M. 2002, MNRAS, 333, 55

Donati, J.-F., Howarth, I.D., Jardine, M.M., Petit, P., Catala, C., Landstreet, J.D., Bouret, J.-C., Alecian, E., Barnes, J.R., Forveille, T., Paletou, F., & Manset, N. 2006, MN-RAS, 370, 629

Evans, N.R., Schlegel, E.M., Waldron, W.L., Seward, F.D., Krauss, M.I., Nichols, J., & Wolk, S.J. 2004, ApJ, 612, 1065

Feldmeier, A., Oskinova, L., & Hamann. W.-R. 2003, A&A, 403, 217

Gagné, M., Oksala, M.E., Cohen, D.H., Tonnesen, S.K., ud-Doula, A., Owocki, S.P., Townsend, R.H.D., & MacFarlane, J.J. 2005, ApJ, 628, 986; err. 634, 712

Gies, D.R., Barry, D.J., Bagnuolo, W.G., Jr., Sowers, J., & Thaller, M.L. 1996, ApJ, 469, 884

Gies, D.R., Mason, B.D., Bagnuolo, W.G., Jr., Hahula, M.E., Hartkopf, W.I., McAlister, H.A., Thaller, M.L., McKibben, W.P., & Penny, L.R. 1997, ApJ, 475, L49

Harvin, J.A., Gies, D.R., Bagnuolo, W.G., Jr.; Penny, L.R., & Thaller, M.L. 2002, ApJ, 565, 1216

Huenemoerder, D. et al. 2009, http://spacebase-alpha.mit.edu/tgcat/

Kahn, S.M., Leutenegger, M.A., Cottam, J., Rauw, G., Vreux, J.-M., den Boggende, A.F.J., Mewe, R., & Güdel, M. 2001, A&A, 365, L312

Kramer, R.H., Cohen, D.H., & Owocki, S.P. 2003, ApJ, 592, 532

Leutenegger, M.A., Owocki, S.P., Kahn, S.M., & Paerels, F.B.S. 2007, ApJ, 659, 642

Li, Q., Cassinelli, J.P., Brown, J.C., Waldron, W.L., & Miller, N.A. 2008, ApJ, 672, 1174

Mewe, R., A. J. J. Raassen, A.J.J., Cassinelli, J.P., van der Hucht, K.A., Miller, N.A., & Güdel, M. 2003, A&A, 398, 203

Miller, N.A., Cassinelli, J.P., Waldron, W.L., MacFarlane, J.J., & Cohen, D.H. 2002, ApJ, 577, 951

Mullan, D.J., & Waldron, W.L. 2006, ApJ, 637, 506

Niemela, V.S., & Gamen, R.C. 2005, MNRAS, 356, 974

Oskinova, L.M., Feldmeier, A., & Hamann W.-R. 2004, A&A, 422, 675

Oskinova, L.M., Feldmeier, A., & Hamann W.-R. 2006, MNRAS, 372, 313

Pellerin, A., Fullerton, A.W., Robert, C., Howk, J.C., Hutchings, J.B., Walborn, N.R., Bianchi, L., Crowther, P.A., & Sonneborn, G. 2002, ApJS, 143, 159

Penny, L.R., Gies, D.R., & Bagnuolo, W.G., Jr. 1996, ApJ, 460, 906

Pollock, A.M.T. 2007, A&A, 463, 1111

Raassen, A.J.J., van der Hucht, K.A., Miller, N.A., & Cassinelli, J.P. 2008, A&A, 478, 513

Rauw, G., Blomme, R., Waldron, W.L., Corcoran, M.F., Pittard, J.M., Pollock, A.M.T., Runacres, M.C., Sana, H., Stevens, I.R., & Van Loo, S. 2002, A&A, 394, 993

Rountree, J., & Sonneborn, G. 1991, ApJ, 369, 515

Rountree, J., & Sonneborn, G. 1993, Spectral Classification with the International Ultraviolet Explorer: An Atlas of B-Type Spectra, NASA RP 1312

Sana, H., Rauw, G., Nazé, Y., Gosset, E., & Vreux, J.-M. 2006, MNRAS, 372, 661

Sanz-Forcada, J., Franciosini, E., & Pallavicini, R. 2004, A&A, 421, 715

Schulz, N.S., Canizares, C., Huenemoerder, D., & Tibbets, K. 2003, A&A, 595, 365

Skinner, S.L., Sokal, K.R., Cohen, D.H., Gagné, M., Owocki, S.P., & Townsend, R.D. 2008, ApJ, 683, 796

Skinner, S.L., Zhekov, S.A., Palla, F., & Barbosa, C.L.D.R. 2005, MNRAS, 361, 191

Smith, M.A., Cohen, D.H., Gu, M.F., Robinson, R.D., Evans, N.R., & Schran, P.G. 2004, ApJ, 600, 972

Smith, M.A., & Fullerton, A.W. 2005, PASP, 117, 13

Stahl, O., Wade, G., Petit, V., Stober, B., & Schanne, L. 2008, A&A, 487, 323

Walborn, N.R. 2009, in Stellar Spectral Classification, ed. R.O. Gray & C. Corbally (Princeton University Press), in press

Walborn, N.R., Fullerton, A.W., Crowther, P.A., Bianchi, L., Hutchings, J.B., Pellerin, A., Sonneborn, G., & Willis, A.J. 2002, ApJS, 141, 443

Walborn, N.R., Nichols-Bohlin, J., & Panek, R.J. 1985, International Ultraviolet Explorer Atlas of O-Type Spectra from 1200 to 1900 Å, NASA RP 1155

Walborn, N.R., Parker, J.Wm., & Nichols, J.S. 1995, International Ultraviolet Explorer Atlas of B-Type Spectra from 1200 to 1900 Å, NASA RP 1363

Waldron, W.L. 2005a, in AIP Conf Proc, X-ray Diagnostics of Astrophysical Plasmas: Theory, Experiment, and Observation, ed. R. Smith (AIP Press: Melville, NY), 774, 353

Waldron, W.L. 2005b, in ASP Conf Ser, The Nature and Evolution of Disks around Hot Stars, ed. R. Ignace & K.G. Gayley (ASP: San Francisco), 337, 329

Waldron, W.L., & Cassinelli, J.P. 2001, ApJ, 548, L45

Waldron, W.L., & Cassinelli, J.P. 2007, ApJ, 668, 456; err. 2008, 680, 1595

Waldron, W.L., & Cassinelli, J.P. 2009, ApJ, 692, L76

Westbrook, O.W., Evans, N.R., Wolk, S.J., Kashyap, V.L., Nichols, J.S., Mendygral, P.J., Slavin, J.D., Spitzbart, B., & Waldron, W.L. 2008, ApJS, 176, 218

Wojdowski, P.S., & Schulz, N.S. 2005, ApJ, 627, 953

Zhekov, S.A., & Palla, F. 2007, MNRAS, 382, 1124

References to Table 1: 1, Evans et al. 2004; 2, Rauw et al. 2002; 3, Burkholder et al. 1997; 4, Gies et al. 1997; 5, Gies et al. 1996; 6, Skinner et al. 2008; 7, Sanz-Forcada et al. 2004; 8, Cohen et al. 2008; 9, Skinner et al. 2005; 10, Niemela & Gamen 2005; 11, Leutenegger et al. 2007; 12, Kramer et al. 2003; 13, Cassinelli et al. 2001; 14, Kahn et al. 2001; 15, Harvin et al. 2002; 16, Miller et al. 2002; 17, Raassen et al. 2008; 18, Pollock 2007; 19, Cohen et al. 2006; 20, Waldron & Cassinelli 2001; 21, Waldron 2005a; 22, Gagné et al. 2005; 23, Schulz et al. 2003; 24, Cohen et al. 2003; 25, Mewe et al. 2003; 26, Li et al. 2008; 27, Waldron 2005b; 28, Smith et al. 2004.

The references in the table are to studies of individual stars, in inverse chronological order for a given star. Analyses of many or most stars in the table have also been presented by Waldron & Cassinelli 2007, Zhekov & Palla 2007, Wojdowski & Schulz 2005, and other references cited in the text.

Table 1.   Stellar and Observational Parameters

Star	Spectral Type	E(B-V)	Normalization Factors[a]	Ne x/ Ne ix	Exp. Time [days]	PI	Refs.
Figures 1 and 3:							
HD 93250	O3.5 V((f+))	0.47	1.08−4/1.92−4/1.56−4	0.72	2.25	Waldron	1
9 Sgr	O4 V((f))	0.35	1.56−4/6.69−4/8.68−4	0.27	1.71	Waldron	2
HD 206267	O6.5 V((f)) + O9.5: V	0.53	1.56−4/3.74−4/7.97−4	0.36	0.86	Schulz	3
15 Mon	O7 V((f)) + O9.5 Vn	0.07	5.45−5/6.58−4/1.74−3	0.08	1.16	Waldron	4
ι Ori	O9 III + ?	0.06	3.41−4/3.42−3/7.26−3	0.18	0.58	Canizares	5
σ Ori AB	O9.5 V + B0.5 V	0.06	1.26−4/2.09−3/4.03−3	0.12	1.06	Skinner	6, 7
β Cru	B0.5 III	0.04	7.62−5/2.10−3/1.15−2	0.08	0.86	Cohen	8
Figures 2 and 4:							
HD 150136	O3.5 If* + O6 V	0.48	5.47−4/9.61−4/9.47−4	0.42	1.04	Skinner	9, 10
ζ Pup	O4 I(n)f	0.06	1.85−3/5.92−3/4.49−3	0.37	0.79	Cassinelli	11, 12, 13, 14
ξ Per	O7.5 III(n)((f))	0.33	1.99−4/1.01−3/1.34−3	0.26	1.84	Massa	$\cdots$
τ CMa	O9 II	0.16	6.09−5/3.53−4/1.44−3	0.18	1.01	Canizares	$\cdots$
δ Ori	O9.5 II + B0.5 III	0.09	4.98−4/3.78−3/9.00−3	0.21	0.57	Cassinelli	15, 16
ζ Ori	O9.7 Ib	0.08	6.82−4/5.52−3/1.02−2	0.22	0.69	Waldron	17, 18, 19, 20
ϵ Ori	B0 Ia	0.08	4.15−4/3.28−3/8.25−3	0.22	1.06	Waldron	21
Figure 6:							
θ^1 Ori C	O7 Vp	0.32	3.68−3	0.87	4.59	Canizares, Gagné	22, 23
τ Sco	B0.2 V	0.04	1.23−2	0.42	0.83	Cohen	24, 25
ζ Oph	O9.5 Vnn	0.32	4.00−3	0.43	0.97	Waldron	26, 27
γ Cas	B0.5 IVe var	0.08	5.72−3	1.64	0.60	Smith	28

[a]Peak emission fluxes in photons s^{-1} cm^{-2} Å^{-1} by which the spectrograms have been divided to normalize them in the plots. The negative powers of ten follow the minus signs. The first value pertains to wavelengths below 11 Å, the second for 11–18 Å, and the third above 18 Å in Figures 3 and 4; whereas, only the largest (or sole) value applies to the entire wavelength ranges in Figures 1, 2, (and 6).

Table 2.   Rest Wavelengths of X-Ray Lines [Å]

| He-like fir Lines					H-like Lines			Strongest Fe XVII Lines		
Ion	IP [eV]	Wavelength			Ion	IP [eV]	Wavelength	Ion	IP [eV]	Wavelength
		r-line	i-line	f-line						
O VII	739	21.602	21.801, 21.804	22.098	N VII	667	24.779, 24.785	Fe XVII	1266	17.096
Ne IX	1196	13.447	13.550, 13.553	13.699	O VIII	871	18.967, 18.973	Fe XVII	1266	17.051
Mg XI	1762	9.169	9.228, 9.231	9.314	Ne X	1362	12.132, 12.138	Fe XVII	1266	16.780
Si XIII	2438	6.648	6.685, 6.688	6.740	Mg XII	1963	8.419, 8.425	Fe XVII	1266	15.996 (blend)
S XV	3224	5.039	5.063, 5.066	5.102	Si XIV	2673	6.180, 6.186	Fe XVIII	1358	16.004 (blend)
					S XVI	3494	4.727, 4.733	O VIII	871	16.006 (blend)
								Fe XVII	1266	15.261
								Fe XVII	1266	15.014
								Fe XVII	1266	12.266
								Fe XVII	1266	12.124 (Ne X blend)
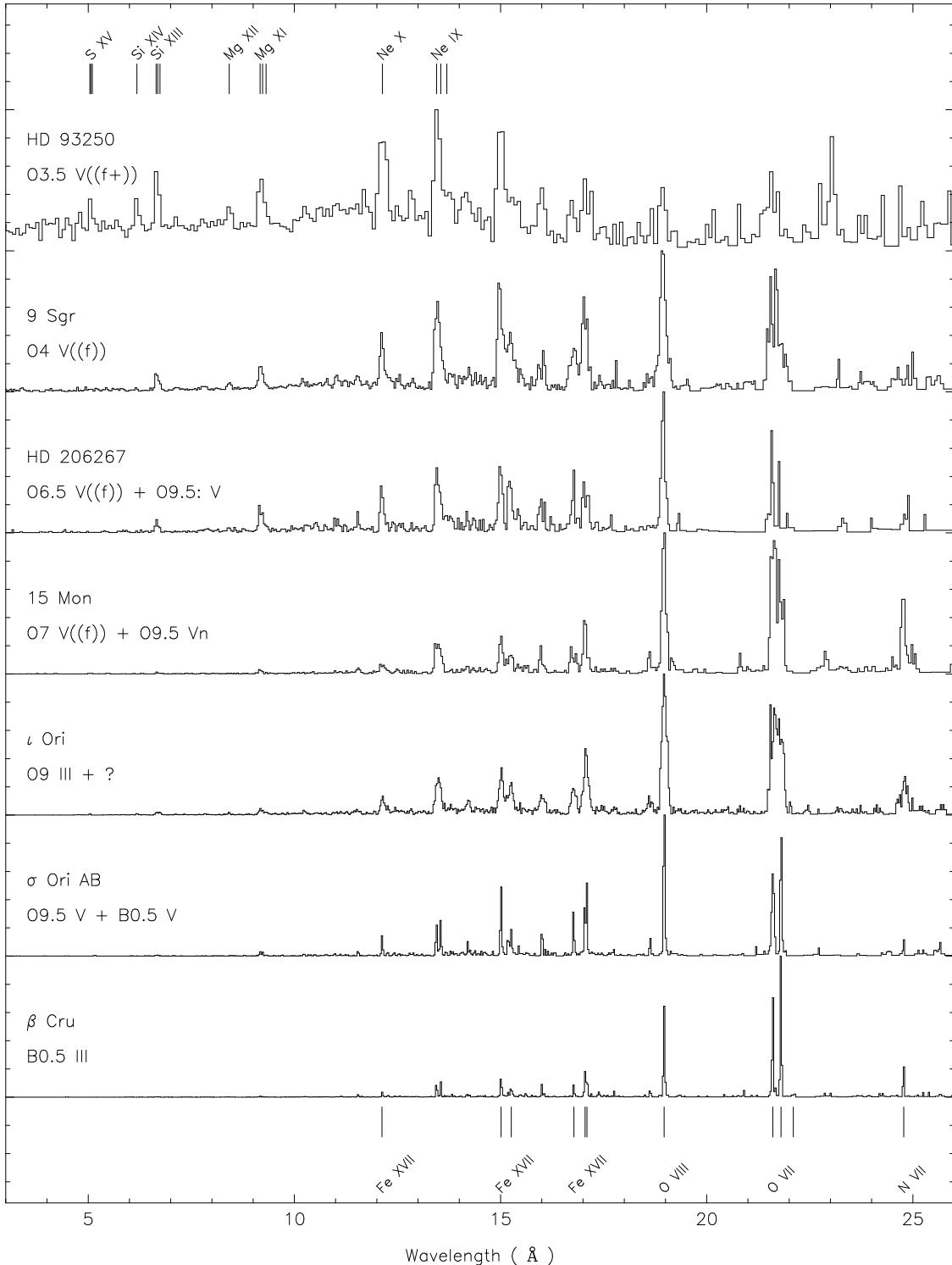
Fig. 1.— X-ray spectral-type sequence of normal dwarfs and giants. The ordinate units are normalized to 1.0 at the peak emission feature in each spectrum, and the corresponding factors are given in Table 1. Thus, this scale may not be intercompared among different spectrograms. The wavelengths of the identified spectral lines are given in Table 2.
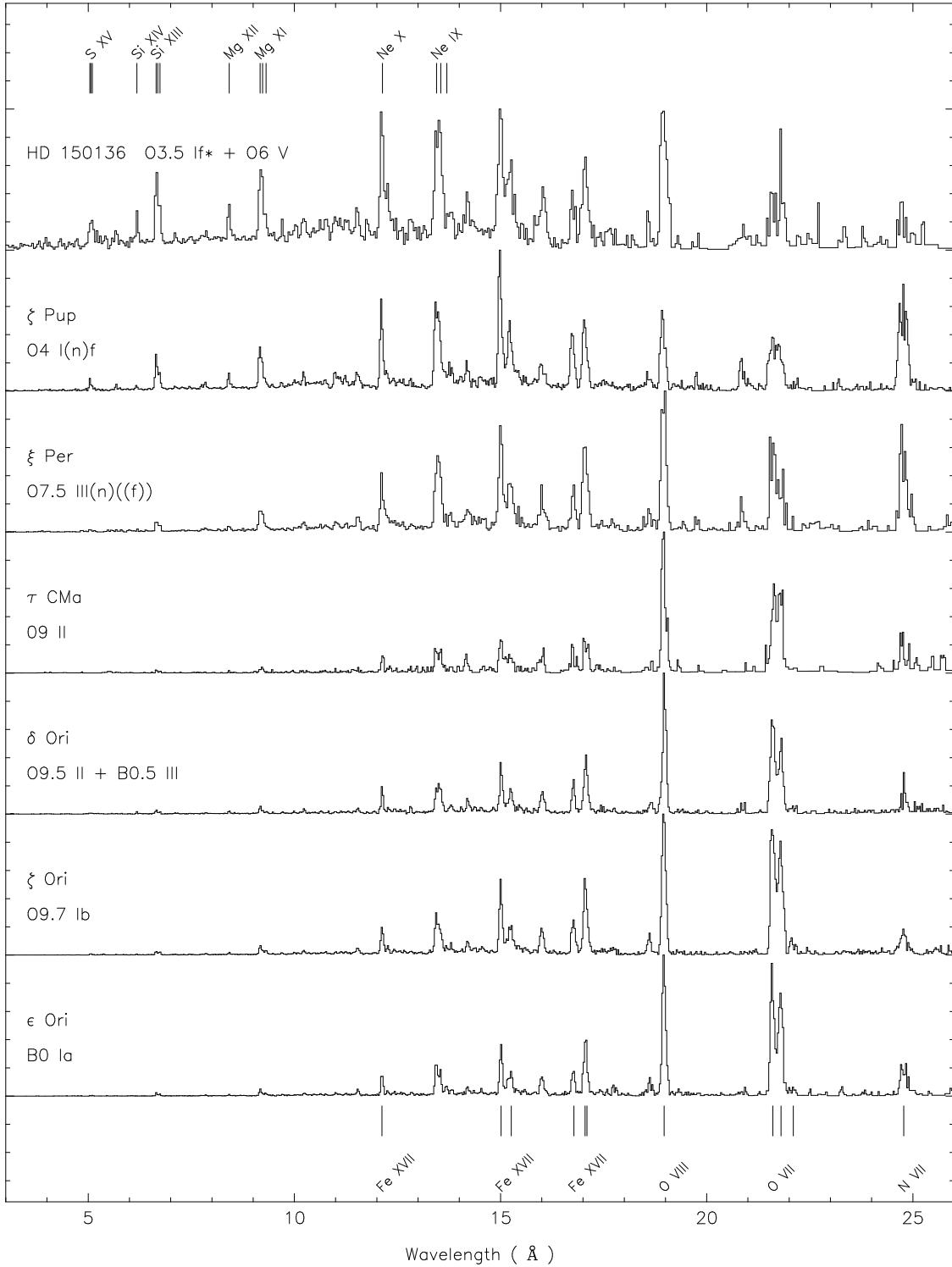
Fig. 2.— X-ray spectral-type sequence of normal supergiants and giants. The ordinate units and the wavelengths of the identified spectral lines are as in Fig. 1.
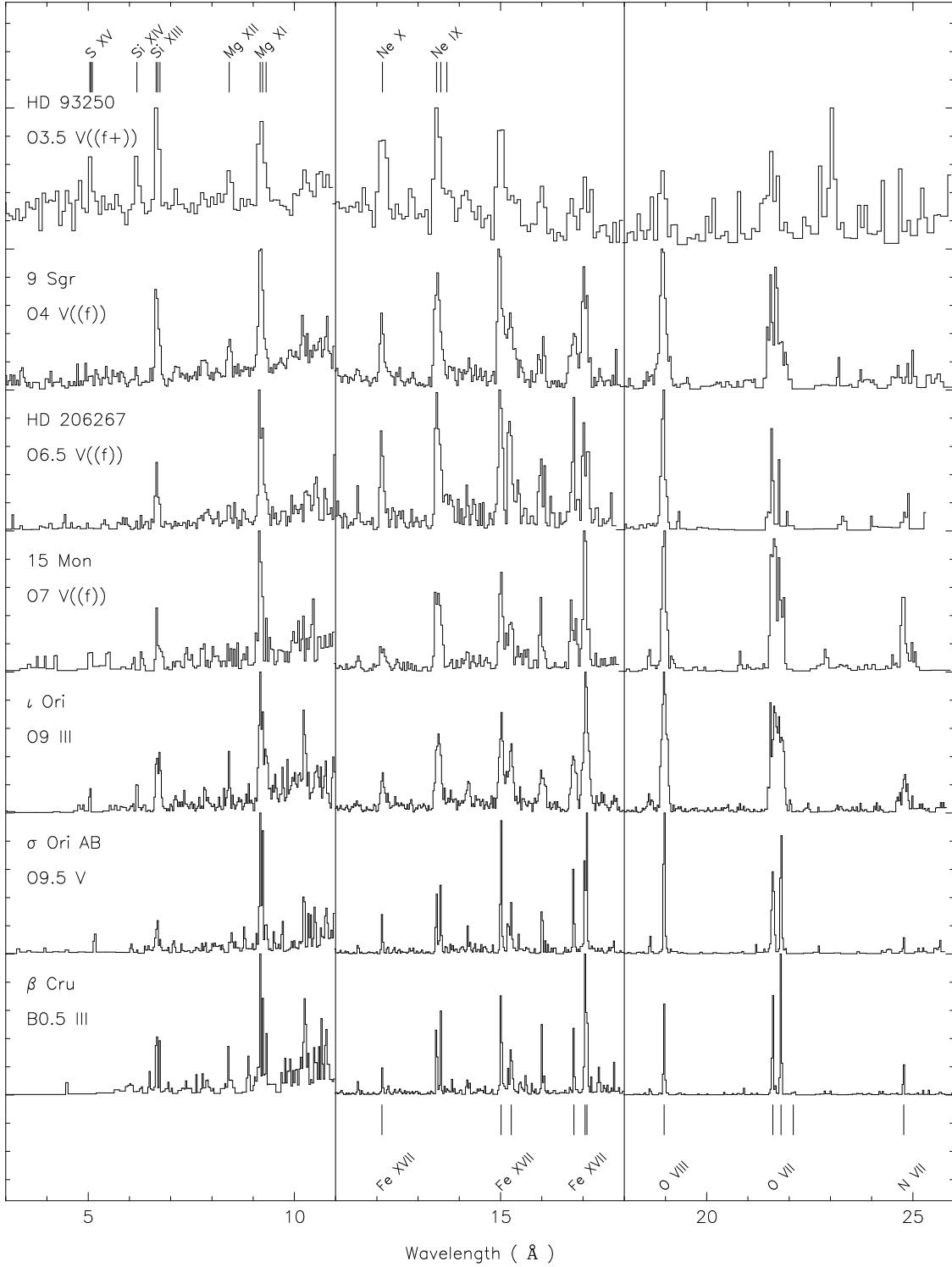
Fig. 3.— The same X-ray spectral-type sequence of normal dwarfs and giants as in Fig. 1, except that the ordinate units are normalized to 1.0 by different factors in each of the three panels, at the peak emission feature in each. The corresponding factors are given in Table 1. The wavelengths of the identified spectral lines are given in Table 2.
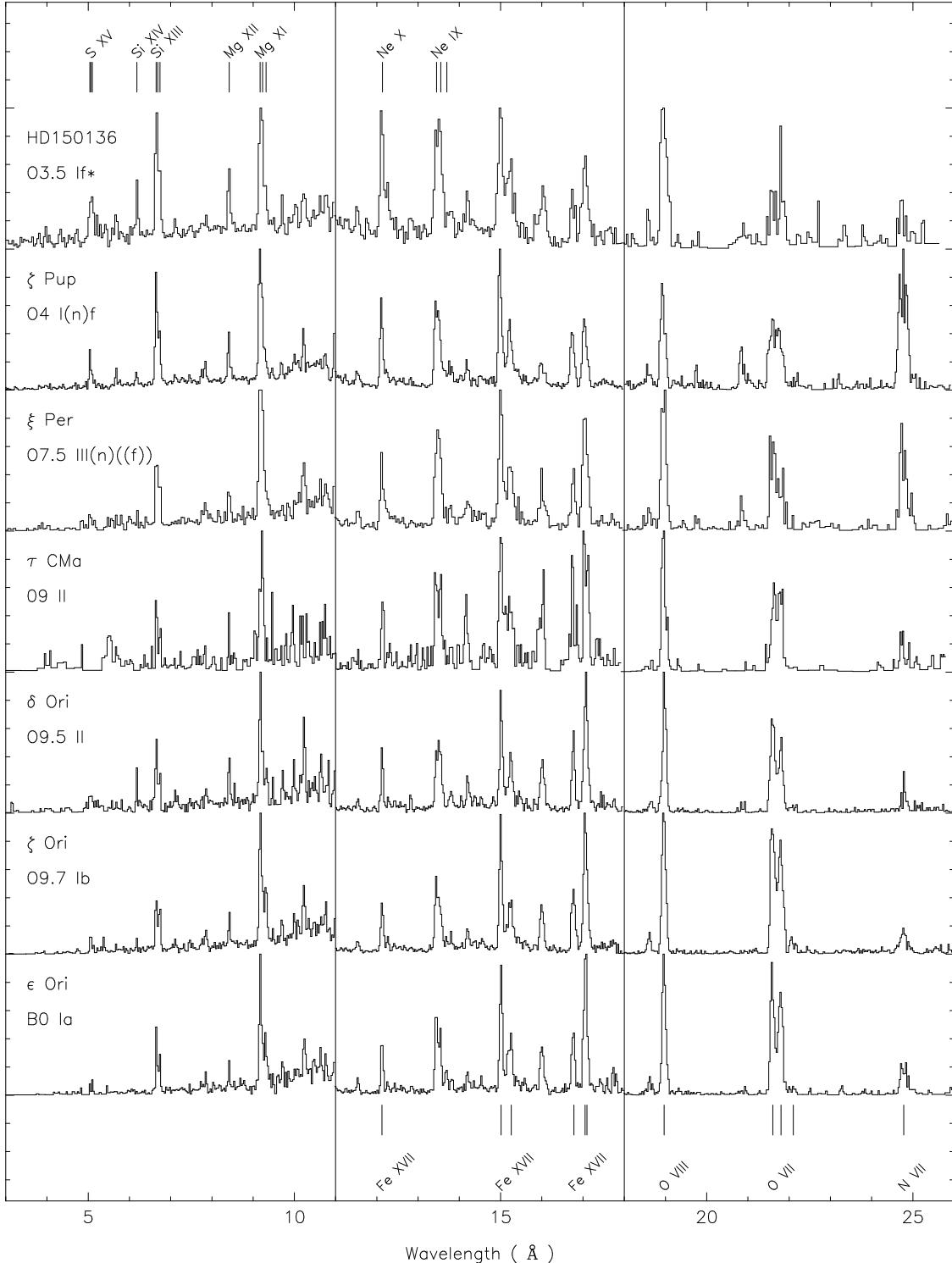
Fig. 4.— The same X-ray spectral-type sequence of normal supergiants and giants as in Fig. 2, except with different normalization factors in each panel, as in Fig. 3. The wavelengths of the identified spectral lines are given in Table 2.
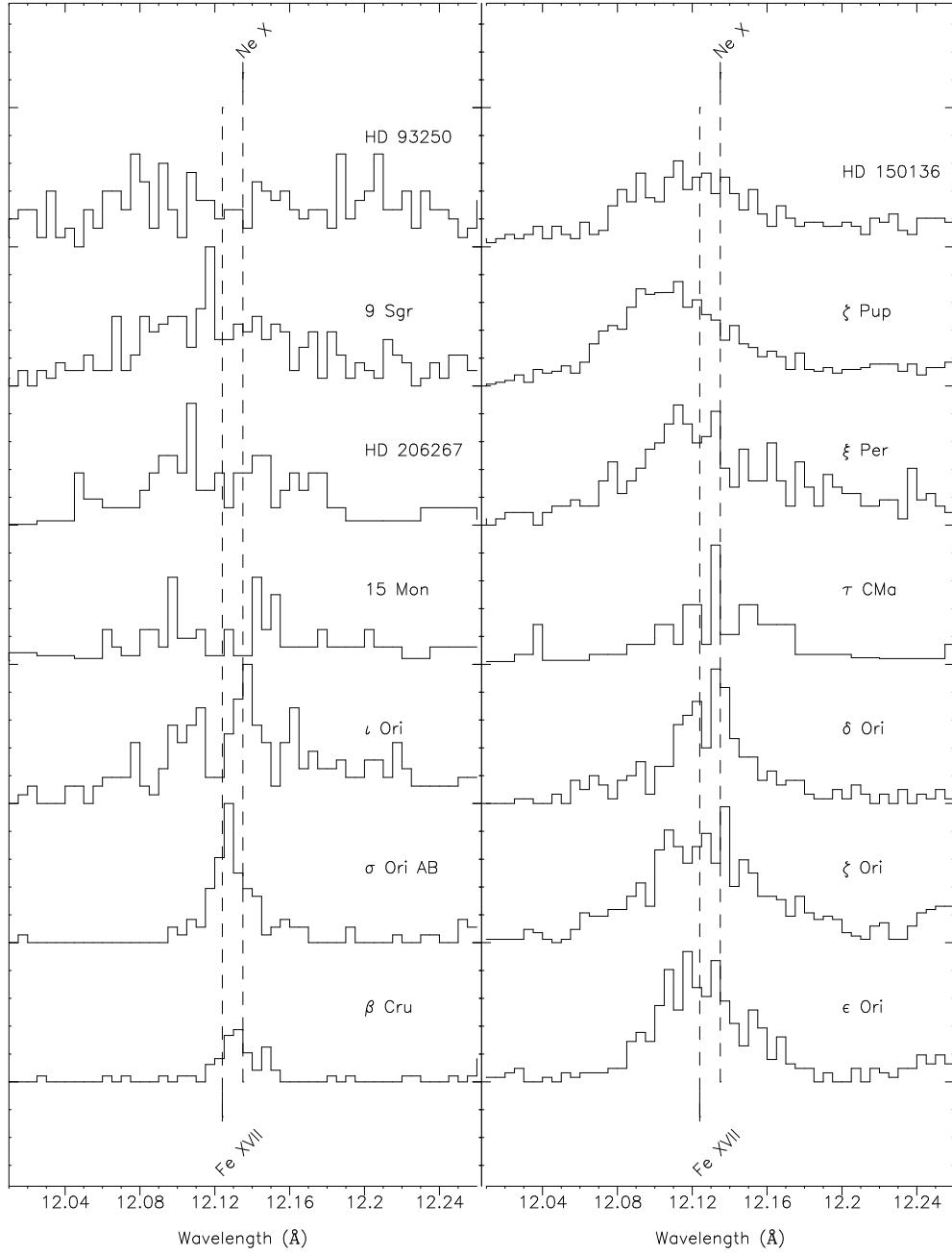
Fig. 5.— An expanded wavelength scale for the Ne X feature, blended with an Fe XVII line, in all the spectra of Figures 1–4. While the two features cannot be resolved, the increasing relative contribution of the Fe line at a slightly shorter wavelength (Table 2) in the later spectral types can be discerned. The Ne feature is very broad in the two earliest dwarfs, and it is blueshifted in the two earliest supergiants.
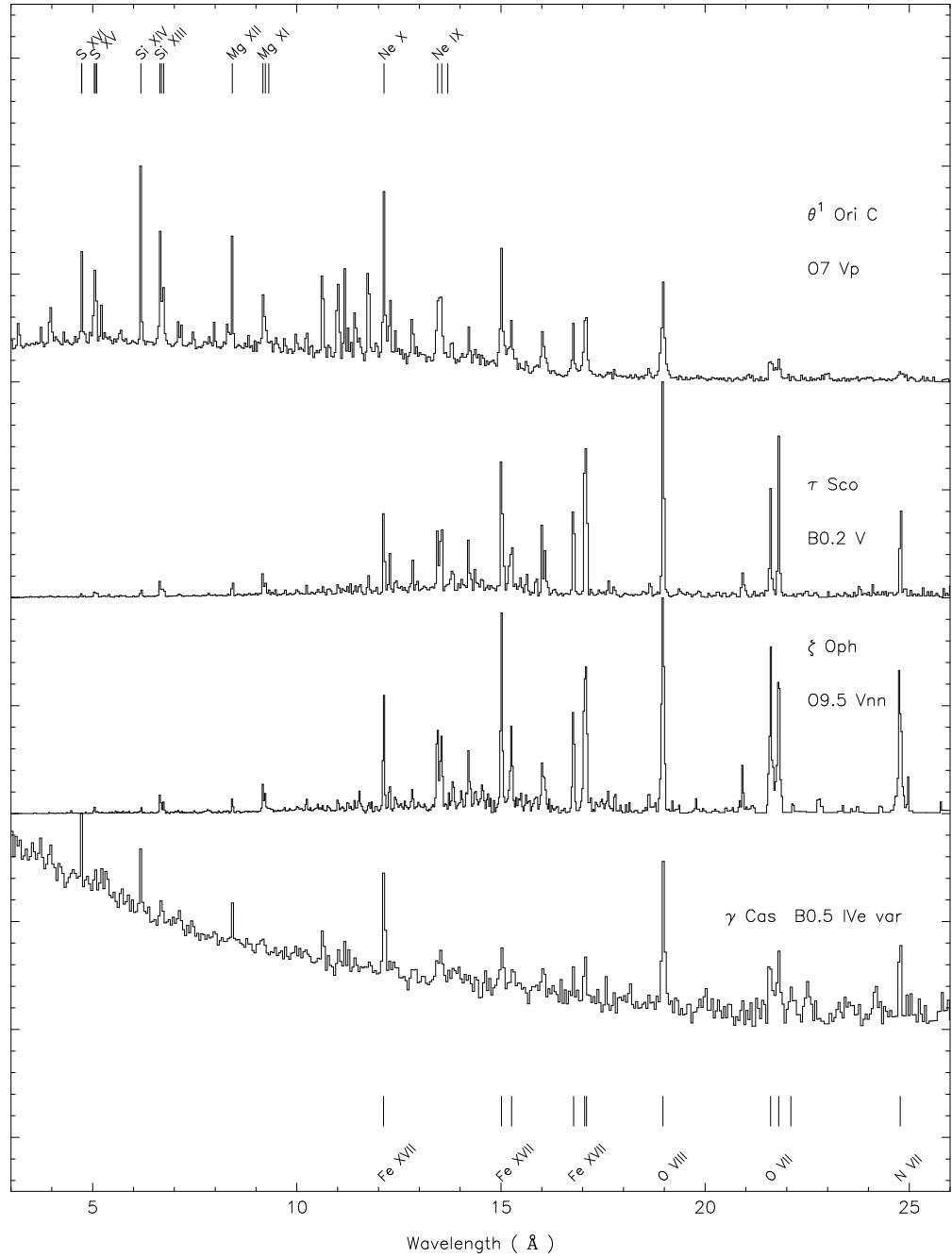
Fig. 6.— X-ray spectrograms of the magnetic stars θ^1 Ori C (Donati et al. 2002, Gagné et al. 2005, Wojdowski & Schulz 2005, Smith & Fullerton 2005, Stahl et al. 2008) and τ Sco (Cohen et al. 2003, Wojdowski & Schulz 2005, Donati et al. 2006); and the rapid rotators ζ Oph (Waldron 2005b, Li et al. 2008) and γ Cas (Smith et al. 2004). The H/He-like line ratios are much larger than in normal stars of the same spectral types. The ordinate units and the wavelengths of the identified spectral lines are as in Fig. 1.
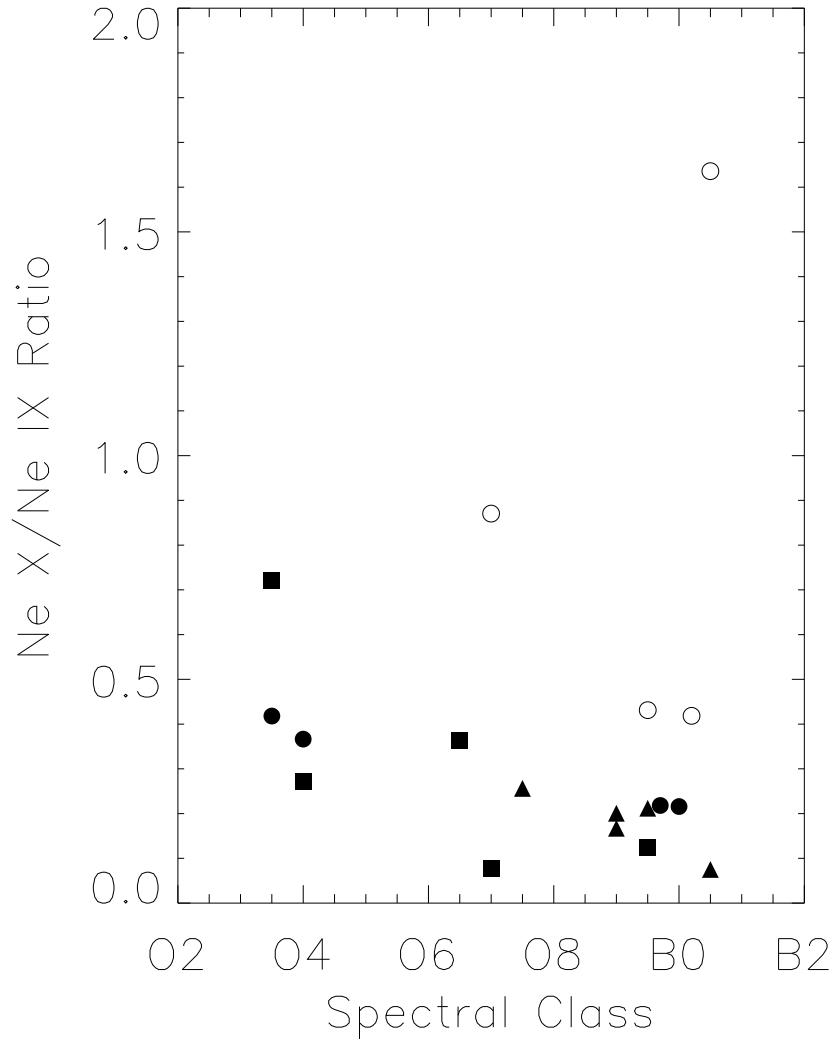
Fig. 7.— Plot of the Ne X/Ne IX ratios, measured as described in the text, as a function of spectral type. The symbols are as follows: *filled squares*, luminosity class V; *filled triangles*, classes III and II; *filled circles*, class I; and *open circles*, peculiar objects. The symbols for ι Ori and τ CMa have been offset by ± 0.018 vertically, to avoid complete superposition (Table 1). The normal stars show a declining ionization trend with advancing type, while the peculiar objects have higher ionization than normal stars of the same types.